Supplementary Materials for

Simultaneous Femtosecond X-ray Spectroscopy and Diffraction of Photosystem II at Room Temperature

Jan Kern, Roberto Alonso-Mori, Rosalie Tran, Johan Hattne, Richard J. Gildea, Nathaniel Echols, Carina Glöckner, Julia Hellmich, Hartawan Laksmono, Raymond G. Sierra, Benedikt Lassalle-Kaiser, Sergey Koroidov, Alyssa Lampe, Guangye Han, Sheraz Gul, Dörte DiFiore, Despina Milathianaki, Alan R. Fry, Alan Miahnahri, Donald W. Schafer, Marc Messerschmidt, M. Marvin Seibert, Jason E. Koglin, Dimosthenis Sokaras, Tsu-Chien Weng, Jonas Sellberg, Matthew J. Latimer, Ralf W. Grosse-Kunstleve, Petrus H. Zwart, William E. White, Pieter Glatzel, Paul D. Adams, Michael J. Bogan, Garth J. Williams, Sébastien Boutet, Johannes Messinger, Athina Zouni, Nicholas K. Sauter, Vittal K. Yachandra*, Uwe Bergmann*, Junko Yano*

*To whom correspondence should be adressed.E-mail: vkyachandra@lbl.gov (V.K.Y.) or bergmann@slac.stanford.edu (U.B.) or jyano@lbl.gov (J.Y.)

This PDF file includes:

Materials and Methods

Sample preparation

PS II was purified from *Thermosynechococcus elongatus* as described elsewhere (*31*). Microcrystals of PS II were obtained by mixing aliquots of the PS II stock solution in buffer A (100 mM PIPES pH 7, 5 mM $CaCl_2$, 0.03% β-dodecyl maltoside (βDM)) at 3-7 mg/ml with equal amounts of buffer B (100 mM PIPES pH 7, 5 mM $CaCl_2$, 3-5% (w/v) PEG 2000) as described previously (*18, 31*). Box shaped crystals (5-15 μm in the longest dimension, 2-5 μm in the shorter dimension, photograph, see ref. 18) were suspended in buffer C (100 mM MES pH 6.5, 5 mM $CaCl_2$, 10% (w/v) PEG2000, 30% (w/v) glycerol). The final concentration of the crystal suspension was determined by measuring Chl concentration of small aliquots of the suspension, dissolved in 80% acetone (*32*). The Chl concentration was adjusted between 0.3 and 0.5 mM, corresponding to a protein concentration of 8.5-14 μM (3-5 mg/ml). For solution samples the purified PS II was resuspended in buffer D (100 mM MES, pH 6.5, 5 mM $CaCl_2$, 0.015% βDM, 1.3 M sucrose) to a final protein concentration of 80-90 mg/ml. The $MnCl_2$ solution measured was 0.5 M Mn in 35% (w/v) glycerol/water as described in (*24*).

Membrane-inlet mass spectrometry (MIMS) measurements

Sample suspensions of PS II from *T. elongatus* of 6 mg/ml chlorophyll were diluted 1:1 with $H_2{}^{18}O$ (97.4%) to give a final enrichment of $H_2{}^{18}O$ of about 48% and final salt concentrations of 5 mM $CaCl_2$, 50 mM MES and 1.2 M Sucrose. No electron acceptors were added. The ^{18}O-enriched samples were loaded into a gas-tight Hamilton syringe and pumped through a silicon capillary (ID = 50 mm, OD 150 mm) into another gas tight Hamilton syringe that collected the sample. Both syringes were placed on separate syringe pumps. Samples were kept in darkness or very dim green light during all steps, except when illuminated inside the capillary with laser light travelling through 1-4 optical fibers (400 mm core diameter) directly attached to a region of the capillary with the polyimide coating removed. This setup directly mirrors the illumination set up for the CXI experiment (see below).

A Nd:YAG laser (Continuum Inlite II-20, 532 nm, 7 ns pulse width) was used for sample illumination. To obtain a stable output intensity of 3.5 μJ/fiber (intensities of individual flashes may vary by ±5%), the laser was operated continuously at 20 Hz and the illumination periods were set with the help of a fast shutter (SH05 operated with SC10 Controller; both Thorlabs).

The oxygen produced was quantified by injecting the illuminated sample into a membrane-inlet system connected via a cooling trap (liquid N_2) to an isotope ratio mass spectrometer (DELTA V, ThermoFinnigan) (*33*). The O_2 formed during illumination was detected with excellent S/N ratio as the non-labeled $^{16}O^{16}O$, the mixed labeled $^{16}O^{18}O$ and double labeled $^{18}O^{18}O$ species. In order to obtain a flash pattern, the light-induced yields for O_2 production (detected at m/z = 34; see Fig. 4a) obtained with (x-1) fibers were subtracted from that with x fibers. For the first flash the background $^{34}O_2$ signal of a non-illuminated sample was subtracted. Each measurement was conducted at least three times.

Sample injection and illumination

Samples were injected into the CXI instrument chamber (*27*) using an electrospun liquid microjet (*25*). Aliquots of 50-150 μl of sample were placed in a microcentrifuge tube placed inside the pressurized cell with a Pt-electrode and the end of the injector capillary submerged in the sample. A pressure of 17 psi against the CXI chamber pressure (10^{-4} Torr) and a voltage of 3000 V was applied on the sample. The injector capillary was a clear silica capillary with inner diameter (ID) of 75 or 100 μm (for the crystal suspensions) or 50 μm (for the solution measurements) and outer diameter (OD) of 360 μm or 150 μm, respectively. The flow rate was in the range of 0.14 μl/min (for the 50 μm ID capillary) to 3.1 μl/min (for the 100 μm ID capillary). To ensure that the samples were in the dark stable S_1 state before injection, all sample handling and storage was performed at darkness or under dim green light. For visualization of the jet an IR laser diode (Coherent Lasiris, 785 nm, 15 mW) was used (see ref. *25* for details). The wavelength was chosen to be outside the absorption spectrum of PS II.

Sample illumination for advancement into higher S-states was conducted using the output of a frequency doubled Nd:YLF laser at 527 nm (Coherent Evolution). The pulse duration of 150 ns was chosen to be much less than 70μs, the $S_1 \rightarrow S_2$ reaction rate, thus preventing the photoreaction from proceeding past the S_2 state.. The light from the laser was coupled into a multi mode fiber light guide with an inner diameter of 400 μm. This light guide was directly coupled onto the silica capillary of the sample injector, allowing illumination of the sample while in the capillary (for more details see the Supplementary material of (*25*)). The flash rate was optimized between 4 and 20 Hz so that at the given flow rate each molecule in the specimen is illuminated once with a flash. The optimum power and flash frequency used was determined by independent O_2 evolution studies (see above and Fig. 4a) and it was sufficient to turnover the S_1 state into the S_2 state. Taking into account the sample flow rate in capillary and jet, and the path length, the time of flight between optical illumination and X-ray probe was Δt = 0.4 to 0.5s, far less than the life time of the S_2 state (half time of >40s).

CXI instrument and X-ray parameters

The CXI instrument of LCLS (*27*) was used in the 1 μm focus setting with the beam being focused to 1.5 × 1.5 μm^2 full width half maximum using Kirkpatrick-Baez mirrors (*34*). The pulse length used was <50 fs (about 45 fs) and the repetition rate was 120 Hz. The energy was varied between 7 and 9.5 keV with $3\text{-}6\times10^{11}$ photons/pulse. The dose therefore varied between 50 and 300 MGray. XRD data were collected using a Cornell-SLAC Pixel Array Detector (CSPAD) (*28,35*). XES was measured using 7 keV excitation, due to the higher cross section for the Mn transition at this energy (note that no differences were found between XES spectra collected at 7 and 9.5 keV excitation (*24*)), XRD was measured at both energies but no difference in diffraction quality between the two energies was observed and the images used for the two data sets were mostly collected at 9.5 keV.

X-ray emission spectroscopy setup

X-ray emission spectra were recorded in a shot-by-shot mode using a custom-built spectrometer in the von Hamos geometry (*23*). The crystal analyzer array was located 500 mm from the interaction point and at an angle of 81° of the center of the array with the X-ray beam. A set of 16 Si(440) crystal analyzers was used and the Bragg angle range was 85.8° to 83.4°, equivalent to an energy range from 6474.6 to 6499.4 eV (limited by the detector size). The signal was recorded on a 140k CSPAD (*29*), located below the interaction region. The setup was calibrated by recording spectra from solutions of $Mn^{II}Cl_2$ and $Mn^{III,IV}$terpyridine as described previously (*24*). This calibration allows for direct comparison between data collected at CXI and data collected using SR sources.

XES at synchrotron sources

For comparison, spectra of PS II solution were collected at BL 6-2 SSRL (Fig. 3c) using an incident energy of 10.4 keV. One spectrum was collected under cryogenic conditions with low dose using a Rowland circle scanning setup and a He cryostat ("SR 8 K intact") and the second one was collected at RT using the von Hamos energy dispersive setup ("SR RT damaged") (*24*). The dose for the low temperature spectrum was 4×10^7 photons/μm^2. The "damaged" RT spectrum was collected using a dose of 3×10^{11} photons/μm^2. This is very similar to the dose applied at CXI in each ultra-short pulse ($2\text{-}3\times10^{11}$ photons/(pulse μm^2)).

X-ray emission data processing

For the PS II S_1 crystal spectrum, the associated diffraction images were initially screened for crystalline diffraction, yielding 19,260 XES detector images where there was a high probability of simultaneous X-ray diffraction (with a hit defined as showing 16 or more strong Bragg spots). For the S_2 crystal spectrum the diffraction images of all potential hits recorded with an incident energy of 7 keV were manually inspected for Bragg spots, yielding a total of 362 crystal hits. Only the XES detector images for these hits were included in the S_2 spectrum. No such initial screening was performed for the S_1 PS II solution spectrum; instead all 375,848 images (equivalent to approximately 52 minutes of data collection time at 120 Hz) were included in the processing.All images were treated initially with a dark current (pedestal) subtraction and corrected for common mode offset. Single-pixel histograms of the recorded pixel values were constructed over all images contributing to the spectrum. Gaussian curves were fitted to the zero and one photon peaks of the histograms, enabling further dark and gain corrections to the histograms directly from the data such that the zero photon peak is centered at zero ADUs (analog-to-digital units) and the separation between the zero and one photon peaks is identical for all pixels. The total count for each pixel was obtained by summing the ADU values above a threshold of 2/3 the separation between the zero and one photon peaks. The final 1D spectra were obtained by integrating the signal in the non-dispersive direction. After integration spectra were smoothed with a moving average over 7 data points (about 0.35 eV), brought to the same background height at 6,500 eV, and normalized to the height of the $K\beta_{1,3}$ peak. For the S_2 crystal spectrum a binning of 5 data points was used to reduce the noise level.

The average volume of sample probed by the X-ray beam is estimated to be 17 μm^3. From this it follows that the total volume of sample probed by X-rays for the S_1 single

crystal spectrum (~20,000 shots, Fig. 3b) is 0.3 nl. The concentration of Mn in the PS II crystals is ~7 mM, therefore the total Mn amount measured for this spectrum is $\sim 2\times10^{-12}$ mol. Accordingly, the Mn amount measured for the S_1 "indexed crystals" (Fig. S4) and the S_2 single crystal spectra (Fig. 4b) are $\sim 1.4\times10^{-13}$ and $\sim 4\times10^{-14}$ mol, respectively. For the PS II solution (c(Mn)=1 mM) the spectrum (Fig. 3b) was obtained from ~375,000 individual shots, equivalent to a total Mn amount of $\sim 6.3\times10^{-12}$ mol.

X-ray diffraction setup and data processing

X-ray diffraction data were recorded using the large CSPAD of the CXI instrument (*28*). Arrangement of the tiles and metrology of the detector were calibrated by measuring a dataset from microcrystals of the protein thermolysin (*25*).

PS II diffraction data were processed with a new software suite (*cctbx.xfel*) that builds upon components developed previously in the synchrotron context for picking Bragg spots (*spotfinder*) and autoindexing (*labelit*) (*36, 37*), using standard methods (*38*) to integrate the intensity, I, of each partial Bragg spot measurement and estimate the individual error, $\sigma(I)$, based on counting statistics. Error estimates from each diffraction pattern were then inflated by assuming that negative intensities are actually decoy measurements (noise only) with a Gaussian distribution centered at zero and with a standard deviation of 1, thus providing a lower bound on modeling errors. Due to this renormalization, $I/\sigma(I)$ values reported here are smaller than those in ref. *18*. Individual reflections were scaled and merged without separately accounting for the partiality fraction of each observation. The quality of the merged reflections was assessed by calculating the correlation coefficient of semi-datasets merged from odd- and even-numbered images ($CC_{1/2}$) as described in ref. *39*.

The structures were solved and refined in *phenix.refine* (*40*) as described previously (*18*). Omit maps were calculated using *phenix.maps,* and map correlations were calculated using *phenix.get_cc_mtz_mtz*.

Supplementary Text

The crystal unit cell varied from batch to batch but no significant variation due to the illumination was visible (see Table 1). When comparing the cell dimensions for XFEL-dark with the 2.9 Å SR structure (*6*) an expansion along the *a* axis by 4%, along the *b* axis by 2% and along the *c* axis by 1.4% are observed. The isomorphism of the XFEL data with the 1.9 Å data (*7*) is reduced as the crystals used for collection of the 1.9 Å data were subjected to a dehydration procedure, leading to a shrinkage of two unit cell axes by about 8% compared to the non-dehydrated crystal form used in the XFEL experiment and for the 2.9 Å data.

The influence of the phasing model on the electron density maps was tested by excluding the non-heme Fe^{2+}, the central four Chl of the reaction center, and the Mn_4CaO_5 cluster. In all three cases clear positive density peaks appear in the omit maps, showing the presence of the respective structural elements from the experimental data (Fig. S2).

To further test the influence of the phasing model on the electron density obtained, the structure factor amplitudes were either shuffled randomly or set to a uniform value of 1. In both cases electron density maps were computed using the 2.9 Å PS II structure (pdb: 3bz1) with the Mn_4CaO_5 cluster omitted as phasing model. No electron density for the Mn_4CaO_5 cluster was observed in both cases (Fig. S3), confirming that the electron density for the oxygen-evolving complex observed when using our experimental structure factors from the XFEL data set is not caused by artifacts from the phasing model.

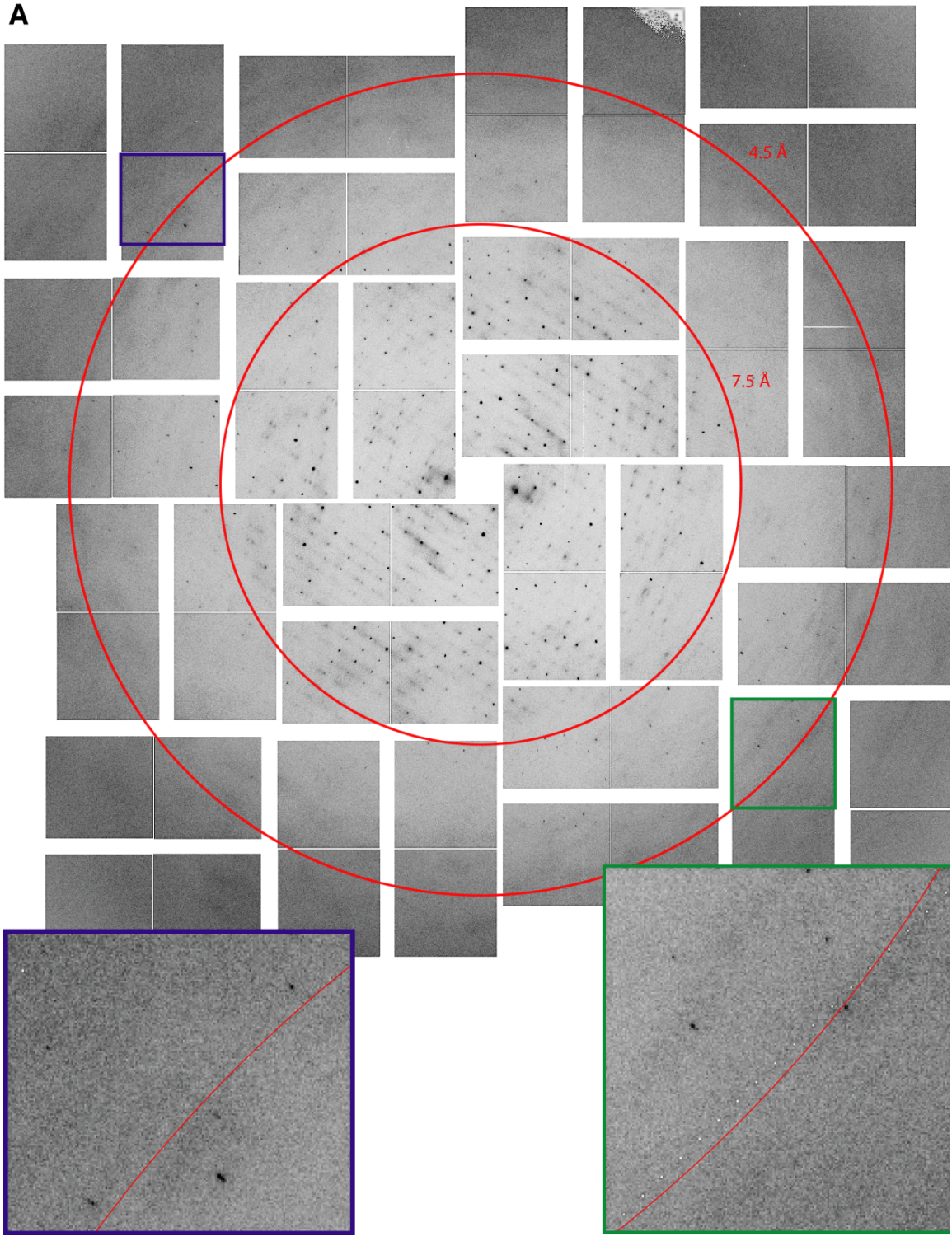
A
4.5 Å
7.5 Å

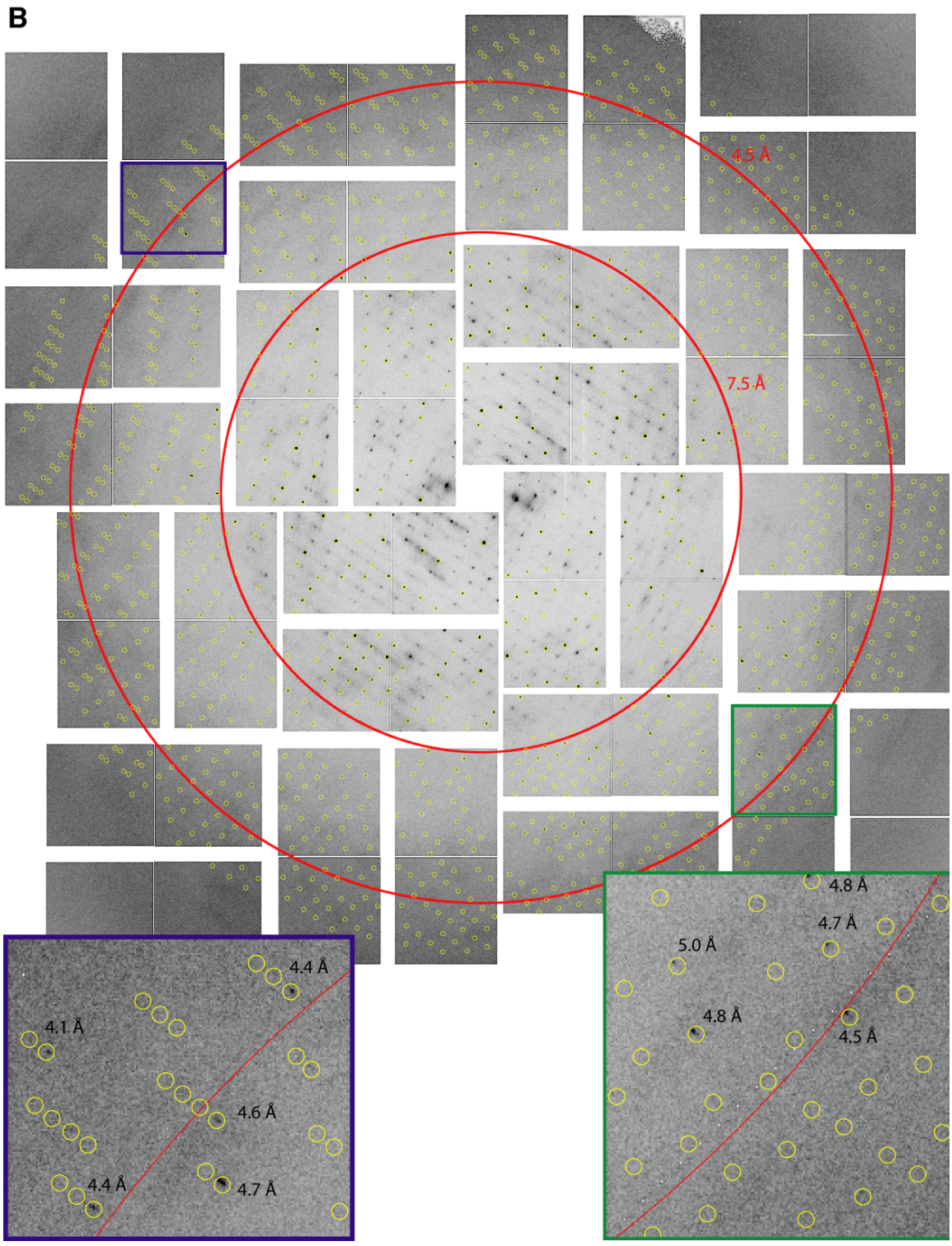
B
4.5 Å
7.5 Å
4.4 Å
4.1 Å
4.6 Å
4.4 Å
4.7 Å
4.8 Å
4.7 Å
5.0 Å
4.8 Å
4.5 Å

Fig. S1.

(A) Diffraction image of a PS II microcrystal recorded at the CXI instrument using a <50 fs X-ray pulse, resolution is indicated at the red rings. Enlarged views of the upper left (blue frame) and lower right region (green frame) of the image are shown in the insets. **(B)** Same diffraction image as in (A), predicted spot positions are shown by yellow rings and resolution of selected spots in the insets are indicated.

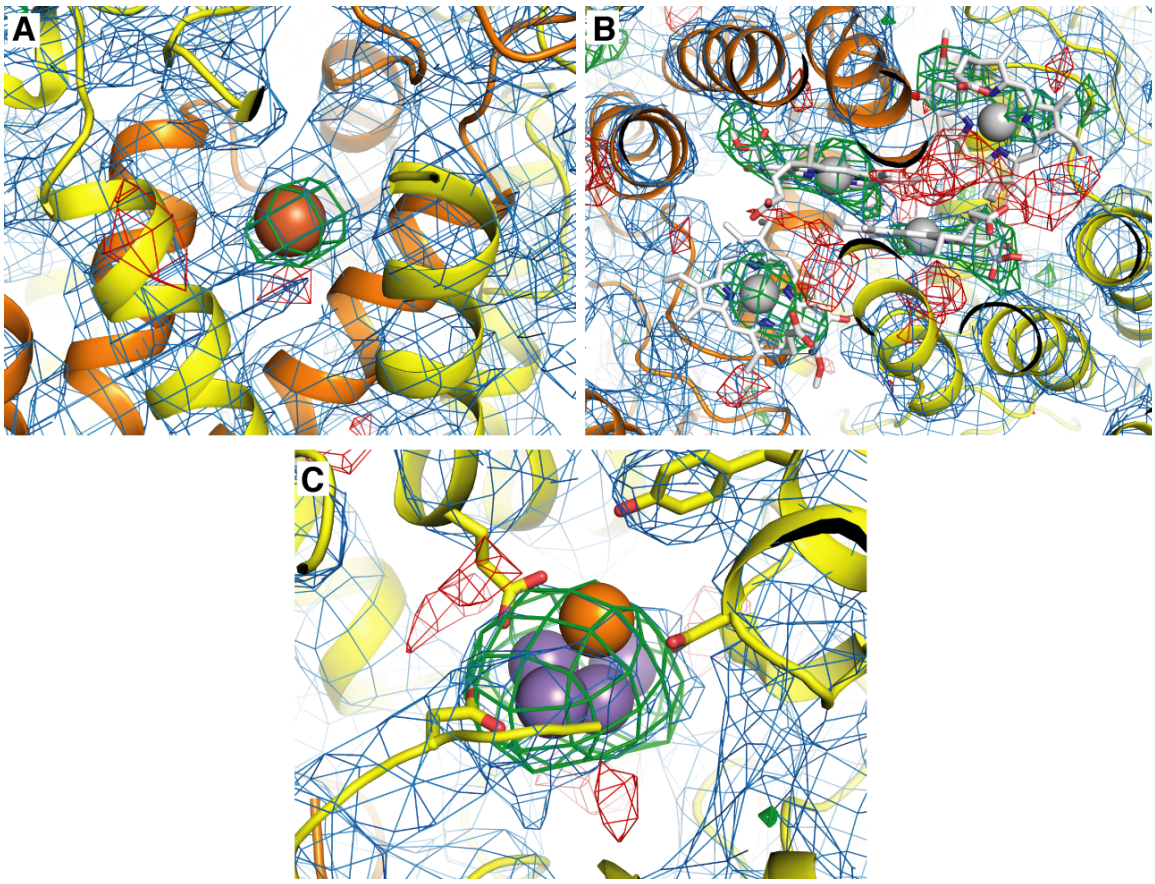

Fig. S2

Separate omit maps obtained by excluding (**A**) the non-heme Fe^{2+}, (**B**) the central four Chl of the reaction center, and (**C**) the Mn_4CaO_5 from the phasing model. $2mF_o-DF_c$ electron density is contoured at 1.0 σ (blue mesh), while mF_o-DF_c difference density is contoured at 2.5 σ (green mesh) and −2.5 σ (red mesh). Observation of difference contours surrounding the omitted atoms is an experimental indication that the atoms are present in the sample at the location observed in conventional SR-based XRD. The protein is shown in yellow (subunit D1) and orange (subunit D2), Fe as a red sphere, Chl as grey sticks with central Mg as grey spheres, Mn as purple spheres and Ca as an orange sphere.

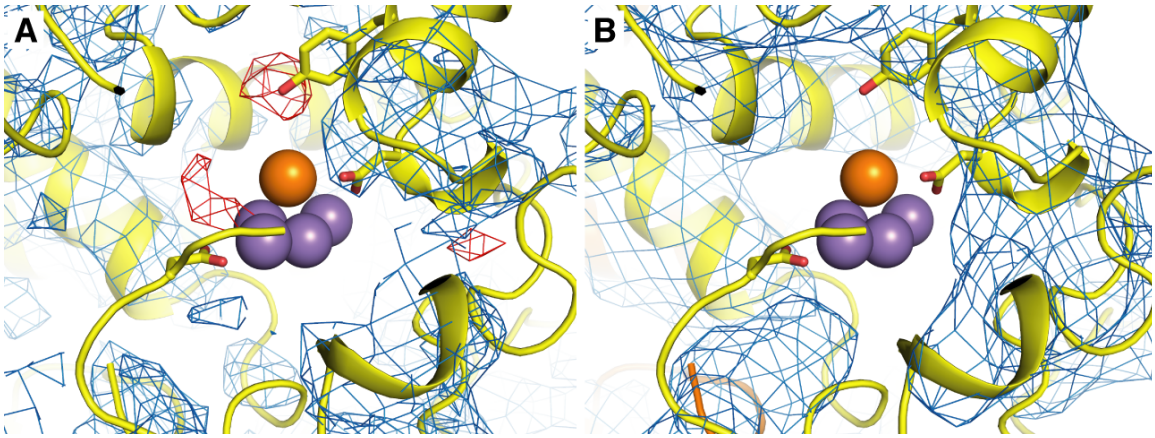

Fig. S3

Phasing controls. Density in the region of the Mn_4CaO_5 cluster obtained by (**A**) shuffling the structure factors F_o or by (**B**) setting them to a uniform value. 2mF_o–DF_c electron density is contoured at 1.0 σ (blue mesh), mF_o–DF_c difference density at 2.5 σ (green mesh) and –2.5 σ (red mesh). Protein is shown in yellow, Mn as purple spheres, Ca as an orange sphere.

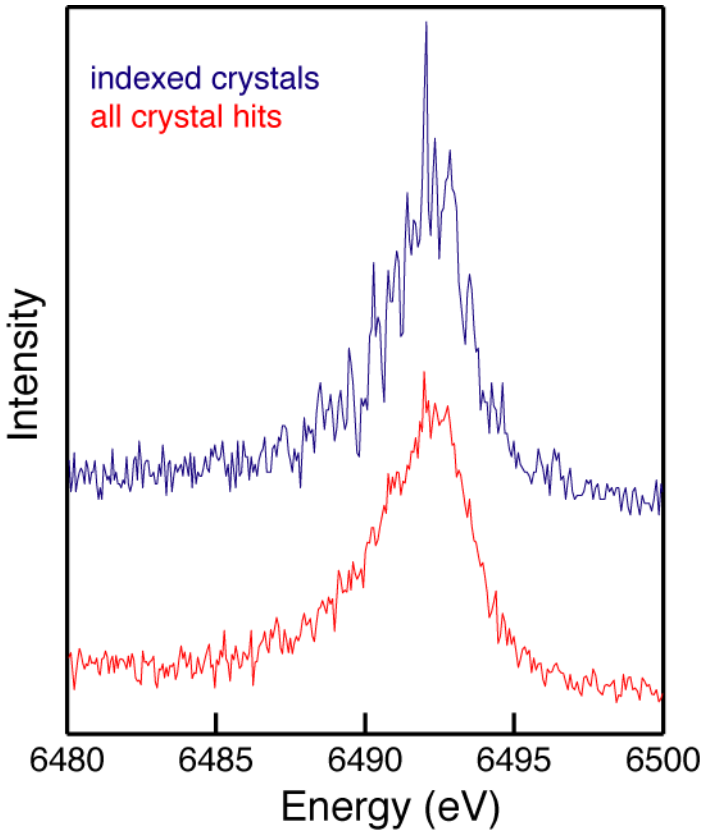

Fig. S4

Raw XES data from PS II microcrystals in the S_1 state recorded at the CXI instrument. The XES data obtained from all 19,260 crystal hits (red) recorded with an incident energy of 7 keV and from the subset of 1362 indexed crystal hits (blue), respectively, are shown (normalized to the same area). Both spectra coincide in the peak position and shape and differ only in the S/N ratio.

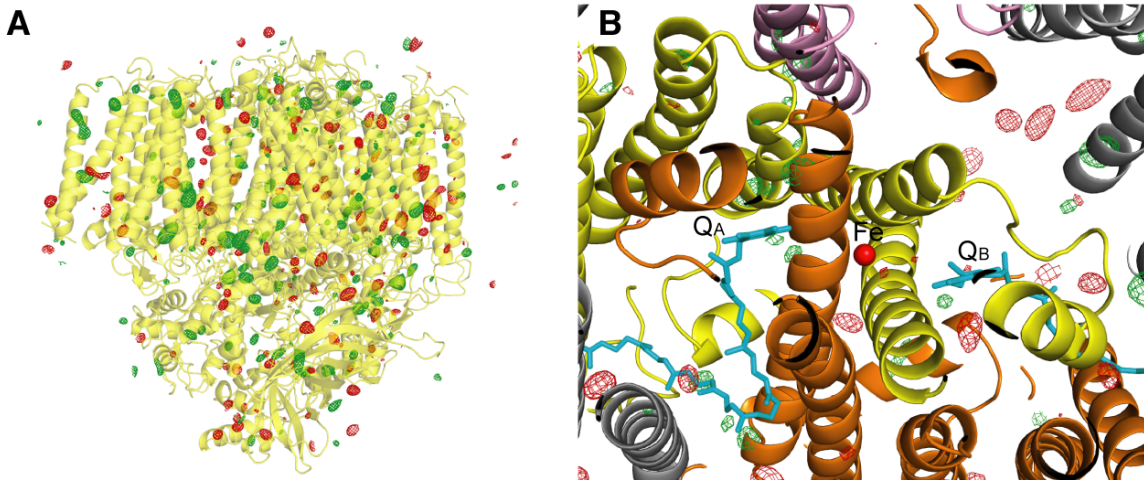

Fig. S5

Isomorphous difference map between the XFEL-illuminated (S_2 state) and the XFEL-dark (S_1 state) XRD dataset; with F_o-F_o difference contours at +3 σ (green) and –3 σ (red); histogram analysis indicates that this map is statistically featureless (Fig. S5). (**A**) View of one monomer of PS II along the membrane plane, with stromal side on top and lumenal side on bottom, protein is shown in yellow. (**B**) View of the electron acceptor side of PS II, located on the stromal side of the complex; view is from the stroma onto the membrane plane. The non-heme Fe is shown as a red sphere, the two quinones Q_A and Q_B as sticks in cyan**,** subunits are shown in yellow (D1), orange (D2), pink (CP43) and grey (others).

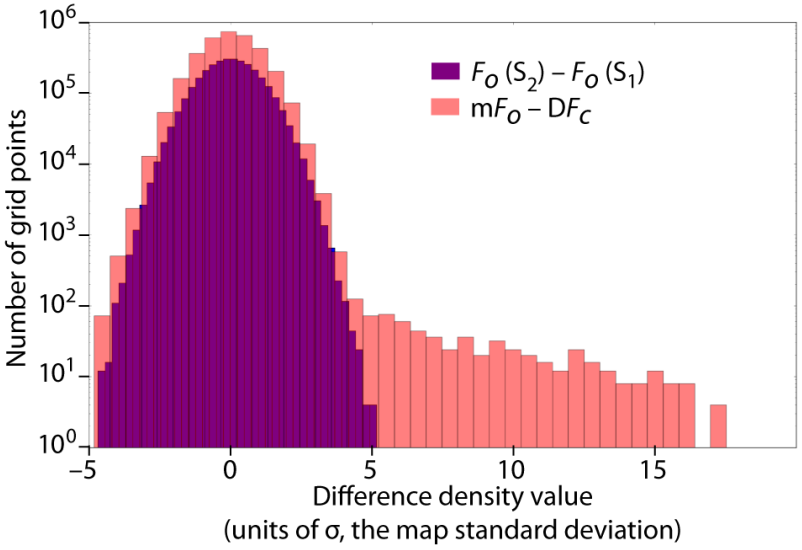

Fig. S6

Histogram analysis of Fourier maps. The distribution of difference density values is plotted for two maps: the XFEL-illuminated (S_2 state) vs. XFEL-dark (S_1 state) F_o-F_o difference map (Figs. 2c and S4, purple); and the Mn_4CaO_5-removed mF_o–DF_c omit map (Fig. S2c, pink). Visual inspection clearly shows that the F_o-F_o resembles a Gaussian function (plotted here on a logarithmic scale) indicating that this difference map is statistically featureless, while the omit map is clearly not featureless (41).

Table S1.
Data collection and refinement statistics.

	Dark (S1 state)	**Light (S2 state)**
Wavelength (Å)	1.2967±0.0012 (N=4436), 1.7546±0.0023 (N=227)	1.2967±0.0017 (N=1833), 1.7547±0.0031 (N=15)
Resolution range (Å)	82.9–5.7 (5.9–5.7)	83.0–5.9 (6.1–5.9)
Space group	P212121	P212121
Unit cell (Å)	131.9±2.5, 227.5±2.2, 307.2±2.7	132.0±2.3, 227.6±2.3, 307.0±2.2
Total reflections	1,475,630 (8,036)	564,722 (8,662)
Unique reflections	27,220 (2,290)	24,671 (2,143)
Multiplicity	54.2 (3.5)	22.9 (4.0)
Completeness (%)	98.3 (85.1)	98.5 (86.5)
Mean I/σ(I)	26.5 (3.3)	22.1 (4.2)
$CC_{1/2}$*	0.802 (0.343)	0.661 (0.376)
R-factor	0.276 (0.320)	0.284 (0.306)
R-free	0.315 (0.350)	0.317 (0.387)
Number of atoms	49,954	49,954
macromolecules	40,772	40,772
ligands	9,182	9,182
Protein residues	5,214	5,214
RMS(bonds)	0.005	0.005
RMS(angles)	1.03	1.02
Ramachandran favored (%)	91	91
Ramachandran outliers (%)	1.4	1.5
Clashscore	23.9	23.5
Average B-factor	81.00	81.10
macromolecules	78.70	78.70

*$CC_{1/2}$ is defined as Pearson's correlation coefficient between two sets, such that for each unique reflection the average intensities of two randomly chosen halves of its independent observations are assigned to different sets (*39*).

Table S2.

Statistics for the XFEL dark state (S_1) data by resolution bins.

Resolution range		# images*	# measurements	# observed unique reflections	Completeness (%)	<Multiplicity>	<I/σ(I)>	$CC_{1/2}$	$n_{1/2}$†
82.95	12.32	4,663	514,385	2,917	100.0%	176.3	98.6	0.851	2,917
12.32	9.78	4,212	306,764	2,785	100.0%	110.2	51.0	0.711	2,785
9.78	8.55	3,740	234,187	2,762	100.0%	84.8	36.8	0.720	2,762
8.55	7.77	3,249	162,201	2,704	100.0%	60.0	22.5	0.656	2,704
7.77	7.21	2,529	104,989	2,753	100.0%	38.1	14.4	0.628	2,750
7.21	6.78	1,814	59,282	2,701	100.0%	22.0	10.2	0.516	2,689
6.78	6.44	1,317	43,616	2,701	99.9%	16.2	7.9	0.526	2,675
6.44	6.16	920	26,288	2,681	99.6%	9.8	5.9	0.418	2,526
6.16	5.93	631	15,778	2,649	98.3%	6.0	4.2	0.300	2,197
5.93	5.72	393	8,838	2,457	92.2%	3.6	3.2	0.353	1,556
5.72	5.54	271	4,833	2,093	77.8%	2.3	2.7	0.370	890
5.54	5.39	165	2,896	1,607	59.9%	1.8	2.5	0.375	454
5.39	5.24	110	1,792	1,188	44.3%	1.5	2.2	0.291	231
5.24	5.12	97	1,601	1,149	42.9%	1.4	2.0	0.316	195
5.12	5.00	95	1,502	1,097	41.1%	1.4	1.9	0.399	180
5.00	4.89	92	1,440	1,035	38.9%	1.4	1.6	0.266	171
4.89	4.80	92	1,405	1,018	37.9%	1.4	1.7	0.334	160
4.80	4.70	79	490	400	15.5%	1.2	1.5	0.244	39
4.70	4.62	8	98	96	3.7%	1.0	1.3	0.000	0
4.62	4.54	8	98	95	3.6%	1.0	1.3	0.000	0
4.54	4.47	8	90	84	3.2%	1.1	1.4	0.000	1
4.47	4.40	6	61	61	2.3%	1.0	1.4	0.000	0
ALL		4,663	1,492,634	37,033	63.7%	40.3	19.9	0.791	27,882

*The number of images is defined as the number of images containing any observations in the indicated resolution range. †$n_{1/2}$ is defined as the number of reflections used in the calculation of $CC_{1/2}$.

Table S3.

Statistics for the XFEL illuminated state (S_2) data by resolution bins.

Resolution range		# images*	# measurements	# observed unique reflections	Complete-ness (%)	<Multi-plicity>	<I/σ(I)>	$CC_{1/2}$	$n_{1/2}$†
82.98	12.32	1,848	184,506	2,913	100.0%	63.3	67.9	0.717	2,914
12.32	9.78	1,682	111,706	2,789	100.0%	40.1	38.0	0.487	2,787
9.78	8.55	1,488	85,458	2,760	100.0%	31.0	28.7	0.562	2,756
8.55	7.77	1,305	61,728	2,708	100.0%	22.8	18.9	0.540	2,698
7.77	7.21	1,077	43,629	2,745	100.0%	15.9	12.4	0.475	2,711
7.21	6.79	847	27,028	2,705	100.0%	10.0	9.0	0.354	2,596
6.79	6.45	674	22,977	2,697	99.5%	8.5	7.3	0.436	2,541
6.45	6.16	543	16,392	2,658	98.9%	6.2	5.3	0.455	2,291
6.16	5.93	422	11,064	2,590	96.3%	4.3	4.0	0.405	1,876
5.93	5.72	272	6,663	2,331	87.2%	2.9	3.1	0.283	1,299
5.72	5.54	213	3,874	1,911	71.4%	2.0	2.6	0.395	680
5.54	5.39	140	2,709	1,561	58.4%	1.7	2.4	0.482	424
5.39	5.24	103	1,961	1,291	48.0%	1.5	2.1	0.344	276
5.24	5.12	93	1,852	1,206	45.0%	1.5	2.0	0.351	274
5.12	5.00	93	1,799	1,219	45.6%	1.5	1.8	0.218	247
5.00	4.89	92	1,564	1,103	41.5%	1.4	1.7	0.348	205
4.89	4.80	88	1,364	1,006	37.4%	1.4	1.6	0.238	164
4.80	4.71	77	473	368	14.1%	1.3	1.5	0.265	40
4.71	4.62	4	51	51	1.9%	1.0	1.6	0.000	0
4.62	4.54	4	45	43	1.8%	1.1	1.5	0.000	1
4.54	4.47	3	42	42	1.7%	1.0	1.2	0.000	0
4.47	4.40	3	18	18	0.7%	1.0	1.9	0.000	0
ALL		1,848	586,903	36,715	62.4%	16.0	15.4	0.665	26,780

*The number of images is defined as the number of images containing any observations in the indicated resolution range. †$n_{1/2}$ is defined as the number of reflections used in the calculation of $CC_{1/2}$.

Acknowledgments

This work was supported by the Director, Office of Science, Office of Basic Energy Sciences (OBES), Division of Chemical Sciences, Geosciences, and Biosciences (CSGB) of the Department of Energy (DOE) under Contract DE-AC02-05CH11231 (J.Y. and V.K.Y.) for X-ray methodology and instrumentation; NIH Grant GM055302 (V.K.Y) for PS II biochemistry, structure and mechanism; Director, Office of Science (DOE) under Contract DE-AC02-05CH11231 (N.K.S.) and NIH Grants R01-GM095887 and R01-GM102520 (N.K.S.) for data processing methods. The DFG-Cluster of Excellence "UniCat" coordinated by the Technische Universität Berlin and Sfb1078, TP A5 (A.Z.), the Solar Fuels Strong Research Environment (Umeå University, J.M.), the Artificial Leaf Project (K&A Wallenberg Foundation, J.M.), VR (J.M.), Energimyndigheten (J.M.) and the Alexander von Humboldt Foundation (J.K.) are acknowledged for supporting this project. The injector work was supported by LCLS (M.J.B., D.W.S.), the AMOS program, CSGB Division, OBES, DOE (M.J.B) and through the SLAC Laboratory Directed Research and Development Program (M.J.B., H.L.). We thank Prof. Ken Sauer for continuing scientific discussions. We thank Pavel Afonine and Nigel Moriarty for refinement advice, Matthias Broser, Selcan Ceylan for support with sample preparation, Christopher Kenney, Ryan Herbst, Jack Pines, Philip Hart, John Morse, Gunther Haller and Sven Herrmann for support with the CSPAD detectors. We thank the staff at LCLS/SLAC for their support and Simon Morton (ALS), Aina Cohen, Mike Soltis (SSRL), Robert Fischetti and Michael Becker (APS) for support of the SR experiments. Experiments were carried out at the LCLS at SLAC National Accelerator Laboratory operated by Stanford University on behalf of DOE, OBES. Testing of crystals and various parts of the setup were carried out at synchrotron facilities which were provided by the Advanced Light Source (ALS), in Berkeley, Stanford Synchrotron Radiation Lightsource (SSRL), in Stanford, and the Advanced Photon Source (APS), in Argonne, funded by DOE OBES. The SSRL Biomedical Technology program is supported by NIH, the National Center for Research Resources, and the DOE Office of Biological and Environmental Research.

Author Contributions

U.B., V.K.Y. and J.Y. conceived the experiment; U.B., J.Y.,V.K.Y., J.K., R.A.-M., J.M., A.Z., N.K.S., G.J.W., S.B., A.R.F.,A.M.,D.M., D.W.S., W.E.W., M.J.B. designed the experiment; R.T., C.G., J.Hellmich, D.D., A.L., G.H., J.K., B.L.-K., S.G., A.Z. prepared samples; S.B., J.E.K., M.M., M.M.S., G.J.W. operated the CXI instrument; M.J.B., H.L., R.G.S., J.K., J.M., B.L.-K., S.G., R.T., C.G., J.Hellmich, J.S., D.W.S., A.M., G.J.W. developed, tested and ran sample delivery system; S.K., J.M. performed O_2 evolution measurements; R.A.-M., J.K., R.T., B.L.-K., S.G., T.-C.W., M.J.L., D.S., J.Y. performed SR XES experiments; R.A.-M., U.B., M.J.B., S.B., N.E., R.J.G., P.G., C.G., S.G., G.H., J.Hattne., J.Hellmich, J.K., J.E.K., H.L., A.L., B.L.-K., D.M., M.M., J.M., N.K.S., M.M.S., J.S., R.G.S., D.S., R.T., T.-C.W., G.J.W., V.K.Y., J.Y., A.Z. performed the LCLS experiment; J.Hattne, N.E., R.J.G., R.A.-M., J.K., R.W.G.-K., P.H.Z., M.M., P.D.A., N.K.S. developed new software and/or processed and analyzed data; J.K., J.Y., J.M., U.B., V.K.Y. wrote the manuscript with input from all authors.